# Solution Structure of the Catalytic Domain of Human Stromelysin-1 Complexed to a Potent, Nonpeptidic Inhibitor

Yu-Chin Li, Xiaolu Zhang, Richard Melton, Vishwas Ganu, and Nina C. Gonnella*

*Novartis Pharmaceuticals Corporation, 556 Morris Avenue, Summit, New Jersey 07901*

*Received June 4, 1998; Revised Manuscript Received August 3, 1998*

ABSTRACT: The full three-dimensional structure of the catalytic domain of human stromelysin-1 (SCD) complexed to a novel and potent, nonpeptidic inhibitor has been determined by nuclear magnetic resonance spectroscopy (NMR). To accurately mimic assay conditions, the structure was obtained in Tris buffer at pH 6.8 and without the presence of organic solvent. The results showed that the major site of enzyme−inhibitor interaction occurs in the S1′ pocket whereas portions of the inhibitor that occupy the shallow S2′ and S1 pockets remained primarily solvent exposed. Because this relatively small inhibitor could not deeply penetrate stromelysin's long narrow hydrophobic S1′ pocket, the enzyme was found to adopt a dramatic fold in the loop region spanning residues 221−231, allowing occupation of the solvent-accessible S1′ channel by the enzyme itself. This remarkable conformational fold at the enzyme binding site resulted in constriction of the S1′ loop region about the inhibitor. Examination of the tertiary structure of the stromelysin−inhibitor complex revealed few hydrogen-bonding or hydrophobic interactions between the inhibitor and enzyme that can contribute to overall binding energy; hence the resultant compact structure may in part account for the relatively high potency exhibited by this inhibitor.

Human stromelysin-1 (MMP-3), a zinc metalloproteinase, is a member of the matrix metalloproteinase family of enzymes which includes the collagenases, gelatinases, matrilysin, and "membrane type" MMPs[1] (MT-MMPs) (*1*−*4*). These enzymes have been implicated in the destruction of cartilage and proteoglycans associated with degenerative diseases such as rheumatoid arthritis and osteoarthritis (*5*, *6*). The MMPs have also been associated with tumor invasion, progression, metastasis, and angiogenesis (*4*, *7*) as well as different aspects of cardiovascular disease such as smooth muscle cell proliferation in restenosis and plaque formation and rupture in atherosclerosis (*8*−*10*). Because of the widespread implications of MMPs in arthritis, cancer, and cardiovascular disease, these enzymes have become important targets for inhibitor design and synthesis (*11*).

Stromelysin is unique among the MMPs because of its involvement in activation of other MMP proenzymes (*6*). The 57 kDa monomeric proenzyme has been cloned and expressed in a C-terminally truncated form of approximately 30 kDa (*12*) which may be subsequently activated via the "cysteine switch" mechanism (*13*) to produce a 19 kDa stromelysin catalytic domain (SCD). This truncated form of the enzyme retains enzymatic activity that is identical to full-length stromelysin in its cleavage of substance-P (*12*) and proteoglycan (*14*). The size, purity, and stability of the stromelysin catalytic domain have made it highly suitable for biophysical studies; hence several tertiary structures of SCD−inhibitor complexes have been solved by either NMR spectroscopy or X-ray crystallography (*15*−*20*). The inhibitors used in these studies, however, were peptidic in nature, and the reported NMR studies were carried out at low pH or in the presence of organic solvent.

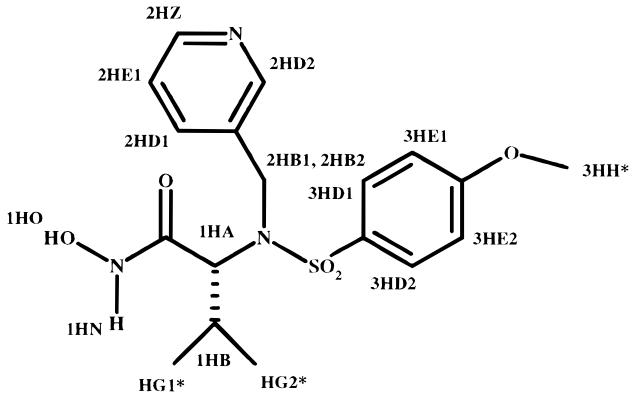


FIGURE 1: Hydroxamic acid inhibitor (CGS 27023) of human stromelysin-1 ($K_i$ = 13 nM). Proton labels are displayed.

Here we report the solution structure of a potent, nonpeptidic inhibitor (CGS 27023) (*21*−*22*) complexed to SCD (Figure 1). These studies were conducted near physiological pH and without the presence of organic solvent. The results showed that the overall global fold of the enzyme is identical to previously reported structures; however a dramatic change occurs in the loop region (residues 221−231) which flanks the S1′ pocket. Our structure revealed an unexpected conformational fold of the enzyme's S1′ loop forming a compact enzyme−inhibitor complex. This conformational fold at the enzyme's binding site may significantly contribute to the overall binding energy of the SCD−inhibitor complex.

* Corresponding Author. Phone: (908) 277-7265. Fax: (908) 277-4435. E-mail: nina.gonnella@pharma.novartis.com.

[1] Abbreviations: SCD, human stromelysin-1 catalytic domain; MMP, matrix metalloproteinase; MT-MMP, membrane type matrix metalloproteinase; COSY, correlated spectroscopy; NOESY, NOE spectroscopy; TOCSY, total correlated spectroscopy; HMQC, heteronuclear multiple quantum correlated; HSQC, heteronuclear single quantum correlated.

S0006-2960(98)01328-2 CCC: $15.00 
Published on Web 09/15/1998

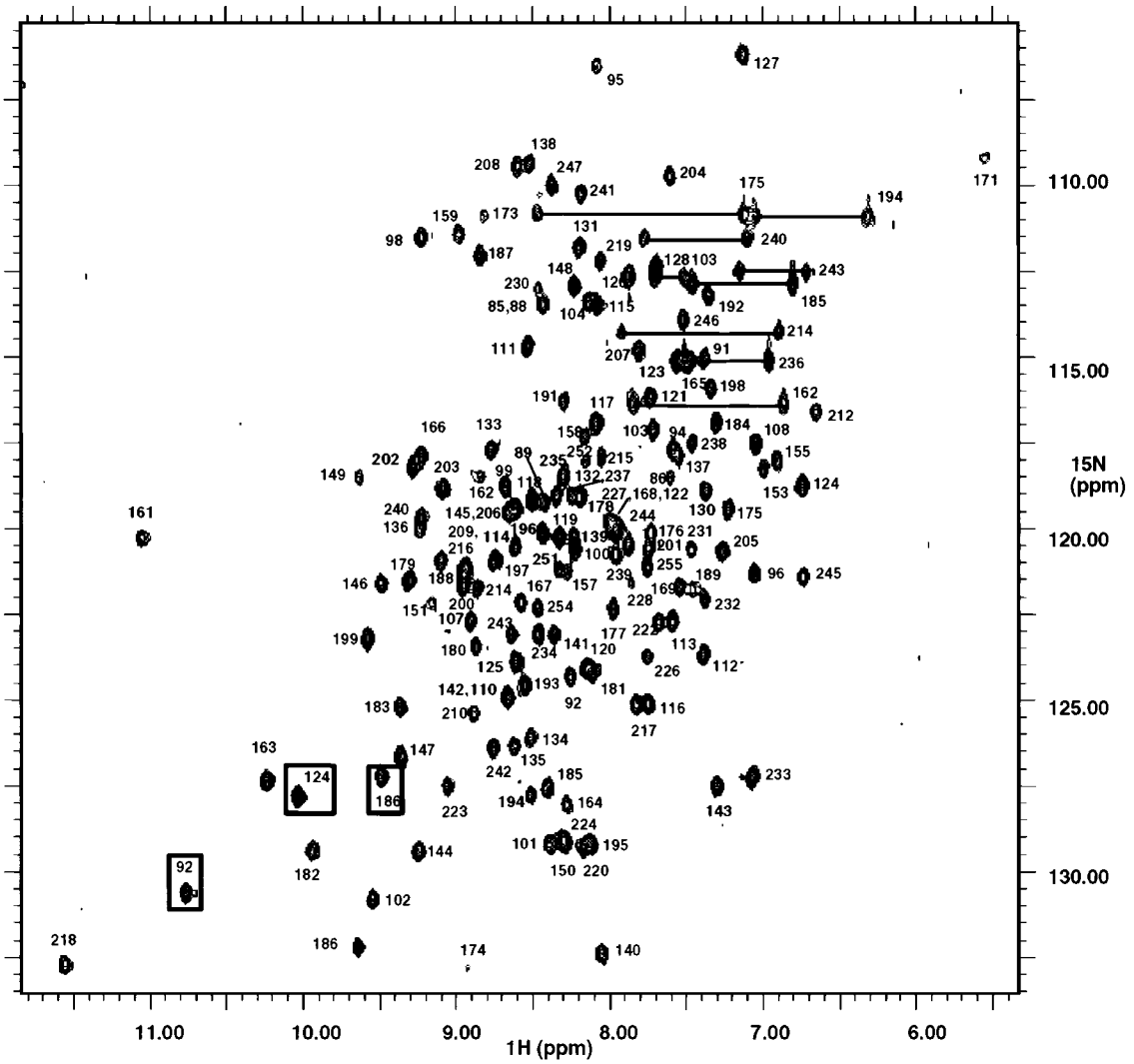


FIGURE 2: Gradient-enhanced $^{15}$N-HSQC spectrum at 14.09 T of the inhibited $^{15}$N-stromelysin catalytic domain (SCD) in buffer (20 mM $Tris_{d11}$−HCl, 20 mM $CaCl_2$, 0.02% $NaN_3$, 90% $H_2O$/10% $D_2O$, pH 6.8). The assigned peaks are indicated by residue numbers (Table 2). Peaks in the boxed regions correspond to tryptophan ring resonances.

In addition, these results stress the importance of incorporating enzyme dynamics into inhibitor docking algorithims to attain a more accurate prediction of inhibitor binding modes.

## MATERIALS AND METHODS

*Sample Preparation of $^{15}$N and $^{13}$C/$^{15}$N-labeled Stromelysin*. Recombinant BL21(DE3) *Escherichia coli* containing the plasmid specifying truncated pro-stromelysin was grown in M9 minimal media using 96% $^{13}$C-6 glucose and/or 99% $^{15}NH_4Cl$ as the main carbon and nitrogen sources, respectively. The media was further supplemented with 0.5 g/L $^{15}$N or $^{13}$C/$^{15}$N algal hydrolysate (Cambridge Isotopes, Woburn, MA). Solubilized pro-stromelysin was purified according to published procedures (*12*). The protein was subsequently activated by heating the sample at 52 °C for 4 h. The activated stromelysin was further purified using a Mono S column eluting with 20 mM MES buffer (pH 6.5), 5 mM $CaCl_2$, and 0.02% $NaN_3$. Pure activated stromelysin was obtained from wash fractions. Electrospray mass spectrometry for $^{15}$N-labeled SCD found a mass of 19 602 Da (91% $^{15}$N label incorporation), theoretical mass is 19 623 Da; and for $^{15}$N,$^{13}$C-labeled SCD a mass of 20 478 Da (97% $^{15}$N,$^{13}$C label incorporation), theoretical mass is 20,505.

*NMR Sample Preparation*. The NMR samples were prepared by concentrating protein to 0.5−1.0 mM. The enzyme was inhibited with 2 mM CGS 27023, and excess inhibitor was removed using Centricon filtration with exchange buffer (20 mM $Tris_{d11}$−HCl, 20 mM $CaCl_2$, 0.02% $NaN_3$ in 90% $H_2O$/10% $D_2O$ or 100% $D_2O$, pH 6.8). The stromelysin catalytic domain (SCD) formed a stable complex with CGS 27023 which remained stable at temperatures up to 45 °C. Denaturation was observed at temperatures exceeding 50 °C by loss in spectral quality and protein precipitation. $^1$H,$^{15}$N-HSQC spectra, which showed excellent resolution and peak dispersion for the SCD−inhibitor complex, provided a facile means of monitoring sample purity, stability, and enzyme integrity (Figure 2).

Sample concentrations typically ranged from 0.5 to 0.7 mM. Concentrations exceeding 1 mM produced significantly broadened lines (35 Hz for amide protons and for $^{15}$N resonances) as well as short spin−spin relaxation times, $T_2$, (18−23 ms for amide protons), most likely as a result of aggregation effects. Reducing enzyme concentrations to 0.75 mM resulted in longer $T_2$ relaxation times (25−30 ms), sharper lines (20 Hz for amide protons and 13 Hz for $^{15}$N resonances), and enhanced peak intensity, affording spectra

Table 1: Constraints Used in Structure Calculation of SCD−Inhibitor Complex

| | |
|---|---|
| total protein−protein NOE distance constraints | 1102 |
| sequential ($\|i - j\| = 1$) | 360 |
| medium range ($2 < \|i - j\| < 4$) | 71 |
| long range ($\|i - j\| > 4$) | 214 |
| intraresidue | 457 |
| total inhibitor NOE distance constraints | 50 |
| inhibitor intramolecular NOE distance constraints | 37 |
| inhibitor−protein NOE distance constraints | 13 |
| total hydrogen-bonding constraints[a] | 208 |
| total metal−ligand distance constraints | 42 |
| zinc−nitrogen/oxygen[b] | 32 |
| calcium−oxygen[c] | 10 |
| total dihedral constraints[d] | 145 |
| NOE restraint violations | |
| number > 0.3 Å | $8 \pm 1$ |
| maximum (Å) | $0.42 \pm 0.04$ |
| conformational energies (kcal mol$^{-1}$) | |
| $E_{total}$ | $788 \pm 16$ |
| $E_{bond}$ | $57 \pm 1.5$ |
| $E_{angle}$ | $301 \pm 8$ |
| $E_{NOE}$ | $256 \pm 10$ |
| $E_{vdw}$ | $118 \pm 6$ |
| Cartesian coordinates (rmsd) (Å) | |
| backbone | $0.52 \pm 0.08$ |
| all nonhydrogen | $0.99 \pm 0.08$ |

[a] HN−O, 1.8−2.2 Å; N−O, 2.8−3.2 Å; HN−C, 2.8−3.2 Å, N−C, 3.8−4.2 Å. [b] Planarity of His ring to zinc was incorporated using 30 His to zinc constraints (*20*). Structures were calculated with two zinc−oxygen bonds to the hydroxamic acid inhibitor. [c] Structures were calculated using ten calcium to oxygen constraints where the first calcium is bound to Asp 158 Oδ1, Gly 159 O, Gly 161 O, Val 163 O, Asp 181 Oδ2, and Glu 184 Oϵ2 and the second calcium is bound to Asp 141 O, Gly 173 O, Asn 175 O, and Asp 177 Oδ1 (*16*, *37*). [d] Dihedral restraints include the following: 39 $\phi$ (α-helical, −100 − 20), 106 $\phi$ (loop region, −180 − 0). These standard constraints were incorporated in the calculations to loosely define allowed $\phi$ angles for backbone α-helical and loop regions.

with the required sensitivity and resolution for 3D data collection.

*Biological Assay (Effects of pH and Organic Solvent on Enzyme Activity). pH Effect.* SCD (210 ng) was diluted in 25 $\mu$L of aqueous solution (0.15 M NaCl and 10 mM $CaCl_2$) and added to 75 $\mu$L of buffer (0.1 M MES or Tris, 10 mM $CaCl_2$, 0.005% Brij, 0.02% $NaN_3$). A final 25 $\mu$L, containing 250 $\mu$M of substrate (Arg-Pro-Lys-Pro-Leu-Ala-Phe-Trp) in 20 mM Tris, 10 mM $CaCl_2$, 0.005% Brij, and 0.02% $NaN_3$, was added to complete the reaction volume. The reaction was terminated after 30 min at 37 °C by adding 20 $\mu$L of 0.2 M EDTA. The reaction mixture (50 $\mu$L) was injected onto a RP-C8 column for analysis of product (*23*). This procedure was repeated at pH values ranging from 5 to 9. The results showed that lowering the pH below 6.5 had a deleterious effect in MES buffer resulting in a 45% loss in enzyme activity, although similar experiments with Tris buffer showed no change in enzyme activity.

*Organic Solvent Effect.* A total of 50 $\mu$L of buffer (20 mM Tris, 10 mM $CaCl_2$, 0.005% Brij, 0.02% $NaN_3$) containing acetonitrile (≤12.5% v/v) was mixed with 25 $\mu$L of 250 $\mu$M [S] (Arg-Pro-Lys-Pro-Leu-Ala-Phe-Trp) in the above buffer. Addition of 50 $\mu$L of SCD (210 ng) completed the reaction volume. This brought the acetonitrile concentration to ≤5%. The reaction was terminated after 30 min at 37 °C by adding 20 $\mu$L of 0.2 M EDTA. The reaction mixture (50 $\mu$L) was injected onto a RP-C8 column for analysis of product (*23*). The results showed that addition of acetonitrile resulted in a 20% loss of activity at concentrations greater than 5%.

Hence to preserve enzyme integrity during complex formation, the stromelysin−inhibitor complex was prepared in $Tris_{d11}$ buffer at pH 6.8 and without the presence of organic solvent.

*NMR Spectroscopy*. The NMR spectra were acquired on a Bruker DMX-600 NMR spectrometer at 25 and 37 °C. Proton, carbon, and nitrogen resonance assignments of stromelysin were made from the following experiments: 2D $^1$H,$^{15}$N HSQC (*24*), 2D $^1$H,$^{13}$C HMQC (*25*), 3D CBCA(CO)-NH (*26*), 3D HBHA(CO)NH (*27*), 3D HNCA (*28*), 3D HNHA (*29*), and 3D HCCH-TOCSY (*30*, *31*). Side chain chemical shifts were assigned from the 3D HCCH-TOCSY spectrum, and specific aromatic assignments were obtained from the $^{13}$C-edited NOESY and $^1$H,$^{13}$C HMQC spectra. The inhibitor resonances were assigned from 2D $^{13}$C-filtered COSY and 2D $^{13}$C,$^{15}$N-filtered NOESY spectra (*32*, *33*). Intramolecular NOE assignments for the enzyme were made from 3D $^{15}$N-edited NOESY and 3D $^{13}$C-edited NOESY

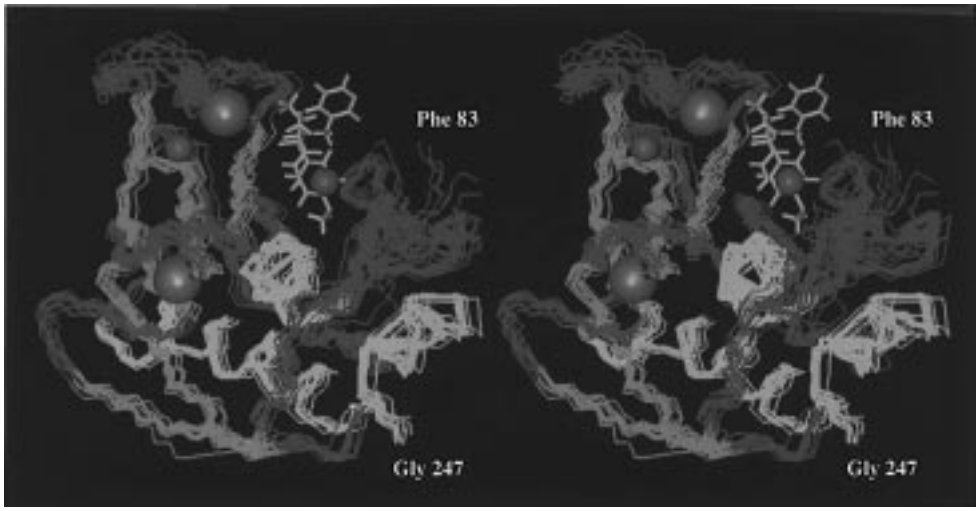


FIGURE 3: An ensemble of 20 structures of the inhibited stromelysin catalytic domain (stereoview, relaxed eye). Backbone residues (Cα trace) from Phe 83 to Gly 247 are displayed. The α-helices appear in green, the $\beta$-sheet regions appear in magenta, and the loops and N-terminus are colored red. The inhibitor is shown in yellow, the blue spheres are zinc atoms, and the gray spheres are calcium atoms.

Table 2: Backbone Chemical Shifts for the Stromelysin−Inhibitor Complex

| residue | $^{1}$HN | $^{15}$N | $^{13}$Cα | Hα | residue | $^{1}$HN | $^{15}$N | $^{13}$Cα | Hα |
|---|---|---|---|---|---|---|---|---|---|
| Phe 83 | | | | | Pro 156 | | | | |
| Arg 84 | | | 55.1 | 4.87 | Phe 157 | 8.27 | 121.1 | 54.4 | 5.00 |
| Thr 85 | 8.44 | 112.5 | 60.3 | 4.83 | Asp 158 | 8.18 | 117.6 | 53.4 | 4.77 |
| Phe 86 | 7.62 | 118.5 | 58.3 | | Gly 159 | 8.99 | 110.4 | 44.2 | 4.41 |
| Pro 87 | | | 61.9 | 4.22 | Pro 160 | | | 63.8 | 3.92 |
| Gly 88 | 8.42 | 112.9 | 44.7 | 3.65/4.18 | Gly 161 | 11.03 | 119.5 | 43.2 | 4.10/3.49 |
| Ile 89 | 8.43 | 118.7 | 61.6 | 3.88 | Asn 162 | | | 55.8 | 4.10 |
| Pro 90 | | | 63.1 | 4.42 | Val 163 | 10.23 | 126.9 | 66.7 | 4.06 |
| Lys91 | 7.39 | 114.3 | 54.4 | 4.53 | Leu164 | 8.30 | 127.6 | 55.3 | 4.57 |
| Trp 92 | 8.26 | 123.8 | 57.7 | 4.46 | Ala 165 | 7.48 | 114.2 | 51.6 | 4.73 |
| Arg 93 | 9.20 | 122.7 | 55.1 | 4.63 | His 166 | 9.27 | 117.1 | 53.9 | 5.09 |
| Lys94 | 7.60 | 117.1 | 53.9 | 4.80 | Ala 167 | 8.59 | 121.6 | 50.8 | 5.10 |
| Thr 95 | 8.08 | 105.2 | 60.8 | 4.38 | Tyr 168 | 8.05 | 119.2 | | 4.25 |
| His 96 | 7.06 | 120.5 | 53.7 | 5.17 | Ala 169 | | | 49.9 | 4.00 |
| Leu97 | 8.31 | 128.6 | 52.5 | 4.57 | Pro 170 | | | 64.0 | 3.08 |
| Thr 98 | 9.26 | 110.5 | 57.9 | 5.87 | Gly 171 | 5.55 | 108.0 | | 3.48 |
| Tyr 99 | 8.66 | 118.1 | 54.6 | 5.75 | Pro 172 | | | 62.4 | 4.79 |
| Arg 100 | 8.22 | 119.9 | 54.8 | 4.39 | Gly 173 | 8.81 | 109.9 | 46.6 | 4.06/3.91 |
| Ile 101 | 8.40 | 128.8 | 61.2 | 4.37 | Ile 174 | 8.93 | 132.9 | 61.7 | 4.26 |
| Val 102 | 9.54 | 130.6 | 65.7 | 3.44 | Asn 175 | 7.22 | 118.7 | 56.2 | 4.20 |
| Asn 103 | 7.72 | 116.3 | 51.1 | 4.77 | Gly 176 | 7.75 | 119.5 | 45.6 | 4.11/4.61 |
| Tyr 104 | 8.16 | 112.5 | 58.5 | 4.29 | Asp 177 | 7.98 | 122.0 | 55.1 | 4.81 |
| Thr 105 | | | 55.6 | 5.02 | Ala 178 | 8.21 | 118.5 | 51.1 | 4.98 |
| Pro 106 | | | 62.8 | 4.69 | His 179 | 9.34 | 121.0 | 50.6 | 5.78 |
| Asp 107 | 8.91 | 122.1 | 55.6 | 4.13 | Phe 180 | 8.90 | 123.0 | 56.5 | 4.34 |
| Leu108 | 7.05 | 117.1 | 50.5 | 4.92 | Asp 181 | 8.15 | 123.6 | 53.4 | 4.42 |
| Pro 109 | | | 62.0 | 4.57 | Asp 182 | 9.95 | 129.1 | 53.0 | 5.59 |
| Lys110 | 8.68 | 124.4 | 60.3 | 3.76 | Asp 183 | 9.37 | 124.7 | 56.5 | 5.05 |
| Asp 111 | 8.54 | 113.8 | 56.4 | 4.40 | Glu 184 | 7.30 | 116.1 | 53.0 | 4.54 |
| Ala 112 | 7.39 | 123.1 | 53.9 | 4.38 | Gln 185 | 8.41 | 127.2 | 53.2 | 4.42 |
| Val 113 | 7.60 | 122.6 | 66.2 | 3.59 | Trp 186 | 9.63 | 132.0 | 56.8 | 5.16 |
| Asp 114 | 8.62 | 120.0 | 57.7 | 4.23 | Thr 187 | 8.81 | 111.2 | 59.8 | 4.97 |
| Ser 115 | 8.08 | 112.6 | 61.3 | 4.29 | Lys188 | 9.08 | 120.2 | 56.6 | 4.61 |
| Ala 116 | 7.73 | 124.6 | 53.3 | 4.26 | Asp 189 | 7.57 | 121.1 | 52.3 | 4.96 |
| Val 117 | 8.09 | 116.1 | 66.9 | 3.32 | Thr 190 | | | 61.5 | 4.69 |
| Glu 118 | 8.51 | 118.4 | 60.1 | 3.76 | Thr 191 | 8.30 | 115.6 | 64.1 | 4.26 |
| Lys119 | 8.34 | 119.7 | 59.4 | 3.99 | Gly 192 | 7.38 | 112.2 | 45.0 | 3.55/4.30 |
| Ala 120 | 8.11 | 123.6 | 55.3 | 4.10 | Thr 193 | 8.55 | 124.1 | 62.4 | 3.76 |
| Leu121 | 7.74 | 115.6 | 57.6 | 3.75 | Asn 194 | 8.49 | 127.5 | 55.3 | 4.85 |
| Lys122 | 7.96 | 119.5 | 58.4 | 4.18 | Leu195 | 8.14 | 128.8 | 57.7 | 4.63 |
| Val 123 | 7.57 | 114.3 | 65.2 | 3.89 | Phe 196 | 8.44 | 119.5 | 61.0 | 4.08 |
| Trp 124 | 6.76 | 118.1 | 57.5 | 4.73 | Leu197 | 8.76 | 120.2 | 57.7 | 3.18 |
| Glu 125 | 8.62 | 123.3 | 59.4 | 4.01 | Val 198 | 7.36 | 115.1 | 65.7 | 4.11 |
| Glu 126 | 7.89 | 111.7 | 58.4 | 4.22 | Ala 199 | 9.59 | 122.7 | 55.8 | 4.18 |
| Val 127 | 7.13 | 104.9 | 59.8 | 4.76 | Ala 200 | 8.96 | 121.0 | 56.5 | 4.07 |
| Thr 128 | 7.69 | 111.4 | 60.1 | 5.58 | His 201 | 7.74 | 119.9 | 58.9 | 4.57 |
| Pro 129 | | | 61.8 | 5.04 | Glu 202 | 9.30 | 117.3 | 58.6 | 4.10 |
| Leu130 | 7.37 | 118.1 | 54.6 | 4.57 | Ile 203 | 9.08 | 118.1 | 61.5 | 3.88 |
| Thr 131 | 8.19 | 110.7 | 59.6 | 4.62 | Gly 204 | 7.60 | 108.6 | 48.0 | 2.45/4.08 |
| Phe 132 | 8.30 | 117.9 | 55.8 | 5.80 | His 205 | 7.27 | 120.0 | 57.0 | 5.71 |
| Ser 133 | 8.77 | 117 | 57.2 | 4.95 | Ser 206 | 8.61 | 118.7 | 55.1 | 4.75 |
| Arg 134 | 8.52 | 125.8 | 55.3 | 3.60 | Leu207 | 7.81 | 114.0 | 54.9 | 4.65 |
| Leu135 | 8.63 | 125.9 | 52.7 | 4.71 | Gly 208 | 8.61 | 108.3 | 44.7 | 3.55/5.01 |
| Tyr 136 | 9.24 | 119.0 | 58.4 | 4.46 | Leu209 | 8.95 | 121.6 | 53.7 | 4.89 |
| Glu 137 | 7.53 | 117.1 | 54.4 | 4.44 | Phe 210 | 8.90 | 124.9 | 53.7 | |
| Gly 138 | 8.52 | 108.3 | 44.2 | 4.14/3.83 | His 211 | 5.30 | | 54.8 | 5.00 |
| Glu 139 | 8.22 | 119.5 | 55.6 | 4.38 | Ser 212 | 6.65 | 115.8 | 56.3 | 4.52 |
| Ala 140 | 8.06 | 132.1 | 49.2 | 4.49 | Ala 213 | 8.58 | 127.0 | 52.0 | 4.67 |
| Asp 141 | 8.35 | 122.6 | 58.5 | 4.57 | Asn 214 | 8.85 | 121.2 | 53.2 | 4.69 |
| Ile 142 | 8.67 | 124.4 | 60.5 | 4.30 | Thr 215 | 8.05 | 117.1 | 63.7 | 2.49 |
| Met 143 | 7.31 | 127.1 | 53.6 | 5.01 | Glu 216 | 8.95 | 120.5 | 55.8 | 4.38 |
| Ile 144 | 9.24 | 129 | 60.5 | 5.42 | Ala 217 | 7.83 | 124.6 | 51.5 | 4.63 |
| Ser 145 | 8.67 | 118.9 | 56.5 | 5.08 | Leu218 | 11.58 | 132.7 | 57.5 | 4.59 |
| Phe 146 | 9.50 | 121.0 | 56.3 | 5.32 | Met 219 | 8.05 | 111.2 | 52.7 | 4.61 |
| Ala 147 | 9.38 | 126.3 | 50.6 | 4.97 | Tyr 220 | 8.17 | 128.8 | 57.3 | 4.80 |
| Val 148 | 8.24 | 111.9 | 59.3 | 5.01 | Pro 221 | | | 62.6 | 3.63 |
| Arg 149 | 9.65 | 117.9 | 56.1 | 3.85 | Leu222 | 7.60 | 122.3 | 54.4 | 4.65 |
| Glu 150 | | | 57.9 | 4.32 | Tyr 223 | 9.07 | 127.2 | 57.9 | 4.61 |
| His 151 | 9.21 | 121.5 | 54.6 | 5.17 | His 224 | 8.28 | 128.5 | 54.2 | 4.83 |
| Gly 152 | 8.49 | 110.3 | 45.8 | 3.58/4.20 | Ser 225 | 7.62 | 118.4 | 58.4 | 4.14 |
| Asp 153 | 6.99 | 117.4 | 50.9 | 4.53 | Leu226 | 7.76 | 123.3 | 54.1 | 4.69 |
| Phe 154 | 8.31 | 117.2 | | 4.24 | Thr 227 | 8.01 | 120.2 | 62.7 | 4.23 |
| Tyr 155 | 6.91 | 117.2 | | 4.91 | Asp 228 | 7.63 | 122.4 | 52.7 | 4.85 |

Table 2 (Continued)

| residue | $^1$HN | $^{15}$N | $^{13}$Cα | Hα | residue | $^1$HN | $^{15}$N | $^{13}$Cα | Hα |
|---|---|---|---|---|---|---|---|---|---|
| Leu229 | 8.87 | 126.8 | 56.7 | 4.19 | Gln 243 | 8.64 | 122.6 | 57.9 | 4.26 |
| Thr 230 | 8.48 | 111.9 | 64.3 | 4.20 | Ser 244 | 7.89 | 119.7 | | |
| Arg 231 | 7.48 | 120.0 | 54.6 | 4.50 | Leu245 | 6.76 | 120.8 | 56.5 | 4.14 |
| Phe 232 | 7.39 | 121.4 | 60.0 | 4.27 | Tyr 246 | 7.50 | 113.0 | 58.4 | 4.88 |
| Arg 233 | 7.08 | 126.9 | 53.9 | 4.02 | Gly 247 | 8.40 | 109.1 | 44.0 | 4.45/4.09 |
| Leu234 | 8.46 | 122.6 | 54.8 | 3.91 | Pro 248 | | | | |
| Ser 235 | 8.34 | 118.4 | 58.1 | 4.57 | Pro 249 | | | | |
| Gln 236 | 9.06 | 122.5 | 58.2 | 3.95 | Pro 250 | | | 62.7 | 4.46 |
| Asp 237 | 8.25 | 118.4 | 58.4 | 4.58 | Asp 251 | 8.33 | 120.5 | 53.9 | 4.65 |
| Asp 238 | 7.46 | 116.8 | 57.5 | 4.73 | Ser 252 | 8.16 | 117.0 | 56.1 | 4.85 |
| Ile 239 | 7.97 | 120.7 | 65.5 | 3.64 | Pro 253 | | | 63.1 | 4.54 |
| Asn 240 | 9.24 | 119.0 | 54.9 | 4.38 | Glu 254 | 8.48 | 121.8 | 56.6 | 4.41 |
| Gly 241 | 8.20 | 109.1 | 45.9 | 2.73/1.41 | Thr 255 | 7.76 | 120.5 | 62.9 | 4.23 |
| Ile 242 | 8.76 | 125.9 | 60.8 | 4.38 | | | | | |

spectra with mixing times of 100 and 150 ms (*34*). Intramolecular NOE assignments for the inhibitor were made from $^{13}$C/$^{15}$N-filtered NOESY spectra acquired at mixing times of 60, 90, 120, 150, and 180 ms. NOE buildup curves were generated for each proton to eliminate those NOEs resulting from spin diffusion effects. Intermolecular NOEs between stromelysin and the inhibitor were assigned from 3D $^{15}$N-edited NOESY and 2D $^{13}$C-filtered NOESY spectra. Hydrogen-bonding constraints, used to define α-helical and $\beta$-sheet regions, were obtained from deuterium-exchange experiments with $^1$H,$^{15}$N HSQC spectra. Hydrogen-bonding interactions between the inhibitor and enzyme were derived from deuterium-exchange experiments with $^{13}$C-filtered NOESY spectra. All 3D data were transformed and processed on a Silicon Graphics (Onyx) workstation using the Felix software (MSI, Burlington, MA), with zero filling in each dimension. All 2D data were processed on a Bruker DMX-600 NMR spectrometer. Data analysis was carried out on Silicon Graphics workstations using NMRCOMPASS software (MSI, Burlington, MA).

*Structure Calculation*. Structure calculations were carried out on a Silicon Graphics Onyx workstation using the X-plor program (*35*). The initial structure of the inhibitor was generated using Quanta (MSI, Burlington, MA). Topology and parameter files for the inhibitor used in the X-plor program were generated from a CHARMm (MSI, Burlington, MA) energy minimized structure. The initial inhibitor structure was then refined against 37 intramolecular NOE constraints using the X-plor program. Randomly sampled structures of SCD were subjected to a previously described simulated annealing protocol (*35*) and refined using 1102 experimentally determined distance constraints and 208 hydrogen-bonding constraints. The refined inhibitor was roughly docked into the enzyme's binding site using Quanta, and the complex was further refined using constraints listed in Table 1. An ensemble of the 20 lowest energy structures superimposed with a combined rmsd of 0.3 Å for backbone secondary structure. All experimental distance constraints were satisfied with no violations > 0.5 Å. Visualization of the calculated structures was performed with Quanta, version 3.2, and InsightII, version 97.0. The atomic coordinates and NOE distance constraints have been deposited with the Brookhaven Protein Data Bank, ID codes 1bm6 and r1bm6mr, respectively.

## RESULTS AND DISCUSSION

*Resonance Assignments.* Over 90% of backbone proton, α-carbon, and nitrogen resonance assignments of the SCD−CGS 27023 complex are listed in Table 2. Proton resonance assignments for the bound inhibitor and intra- and intermolecular NOE assignments defining its bound conformation and binding mode were made as previously described (*36*).

The invariant histidine residues at positions 151 N$\epsilon$2, 166 N$\epsilon$2, and 179 N$\delta$1, which complex the structural zinc and histidines 201 N$\epsilon$2, 205 N$\epsilon$2, and 211 N$\epsilon$2, which complex the catalytic zinc, were assigned as previously reported in both NMR and X-ray studies (*15, 19*). Two octahedrally coordinated calcium ion interactions (Table 1) were also incorporated on the basis of previously reported X-ray data (*16*, *37*).

*Enzyme Structure.* The enzyme secondary structure for the SCD−CGS 27023 complex was identical to that previously reported (*15*−*20*). Three α-helical regions, consisting of helix $\alpha_1$ (residues 110−128), helix $\alpha_2$ (residues 195−208), and helix $\alpha_3$ (residues 235−247) were identified from $d_{NN}$, $d_{\alpha N(i,i+3)}$, and $d_{\alpha N(i,i+4)}$ NOEs which were obtained from the $^{15}$N-edited NOESY spectrum. Likewise $\beta$-sheet strands for $\beta_1$ (residues 95−102), $\beta_2$ (residues 131−135), $\beta_3$ (residues 142−147), $\beta_4$ (residues 164−168), and $\beta_5$ (residues 176−182) were identified from $d_{\alpha N}$ and interstrand $d_{\alpha N(ij)}$ and $d_{NN(ij)}$ NOEs. This secondary structure was supported by deuterium-exchange studies which showed slow exchange for amide protons in the α-helical and $\beta$-sheet regions.

The tertiary fold of the SCD−CGS 27023 complex was calculated from 1152 proton−proton NOE distance constraints (Table 1). These results were in good agreement with previously reported structures (*15*−*20*). An ensemble of 20 structures satisfying the experimentally determined distance constraints is shown in Figure 3. These structures display backbone elements from residue Phe 83 to residue Gly 247 with the N-terminus and loop regions displayed in red, the $\beta$-sheet regions in magenta, and the α-helices in green. While the N-terminus does show some degree of backbone flexibility, it is located near the active site as supported by NOEs from Thr 85 (HA) to Phe 210 (HN), Lys 91 (HD1) to Leu 207 (HN), Trp 92 (HD1) to Leu 207 (HN), Trp 92 (HE1) to Leu 207 (HD2*), and Trp 92 (HN) to Leu 207 (HA). The $\beta$-sheet region is comprised of 4 parallel strands, $\beta_1$, $\beta_2$, $\beta_3$ and $\beta_5$, and one antiparallel strand, $\beta_4$, which extends along the ligand binding cleft. The

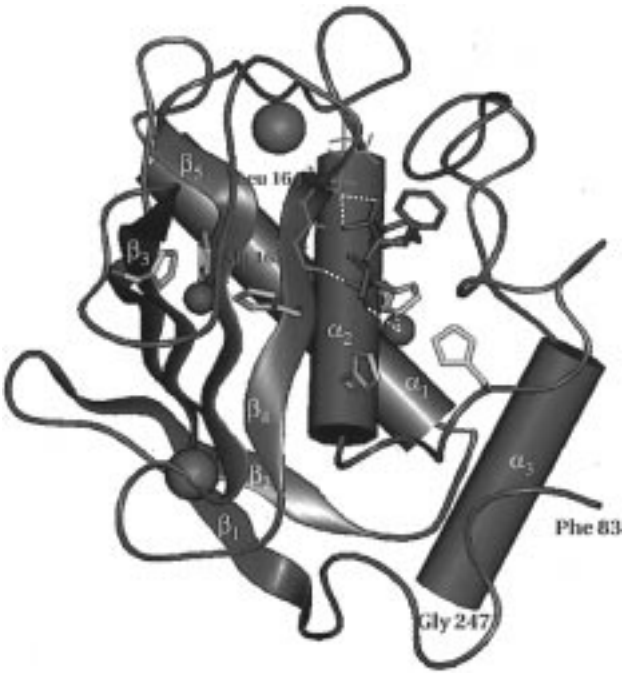


FIGURE 4: Solid diagram of the SCD−CGS 27023 complex with α-helices and β-sheets labeled. The protein backbone (residues Phe 83−Gly 247) is displayed in blue and the inhibitor appears in red. Zinc and calcium atoms appear as purple and orange spheres, respectively. Histidines ligating the catalytic and structural zinc atoms are displayed in yellow. Hydrogen bonds between the Leu 164 amide proton and the inhibitor's sulfonamide oxygens and between the Ala 165 carbonyl oxygen and the hydroxamate amide proton (1HN) and electrostatic interactions between the catalytic zinc atom and the hydroxamate oxygens are shown as dotted white lines.

amphipathic helix $\alpha_1$ separates $\beta_1$ and $\beta_2$ and extends along the full length of the protein. Helices $\alpha_2$ and $\alpha_3$ follow strand $\beta_5$ with helix $\alpha_2$ forming one side of the active site cleft. Histidines 201 and 205 on helix $\alpha_2$ and histidine 211 from the connecting loop region ligate the catalytic zinc. The structural zinc, which has been reported to exist only in the isolated catalytic domain (*38*), is coordinated by His 166 on $\beta_4$, His 179 on $\beta_5$, and His 151 on the loop joining strands $\beta_3$ and $\beta_4$ (Figure 4). Evaluation of the calculated ensemble of structures using PROCHECK (*39*) showed satisfactory peptide bond planarity and Cα chirality. The Ramachandran map showed 94.5% of the nonglycine and nonproline residues in allowed regions. Approximately 4.9% of the residues were in marginally allowed regions, and only 0.7% were in disallowed regions.

*Comparison of Inhibitor Binding.* The inhibitor, CGS 27023, is a hydroxamic acid whose major site of enzyme interaction is the S1′ pocket. As shown schematically in Figure 5A, this inhibitor adopts a conformation in the bound state where the methoxy phenyl ring penetrates S1′, the pyridine ring occupies the shallow S2′ pocket, and the isopropyl ring points toward S1. Both the pyridine ring and the isopropyl groups are primarily solvent exposed. The only portion of the molecule making any significant hydrophobic contact with the enzyme is the methoxyphenyl group. Upon generating structures using only NOE distance constraints, two distinct hydrogen-bonding interactions became apparent; the first between the carbonyl oxygen of Ala 165 and 1HN of the hydroxamic acid (2.15 Å) and the second between the amide proton of Leu 164 and the inhibitor's sulfonamide

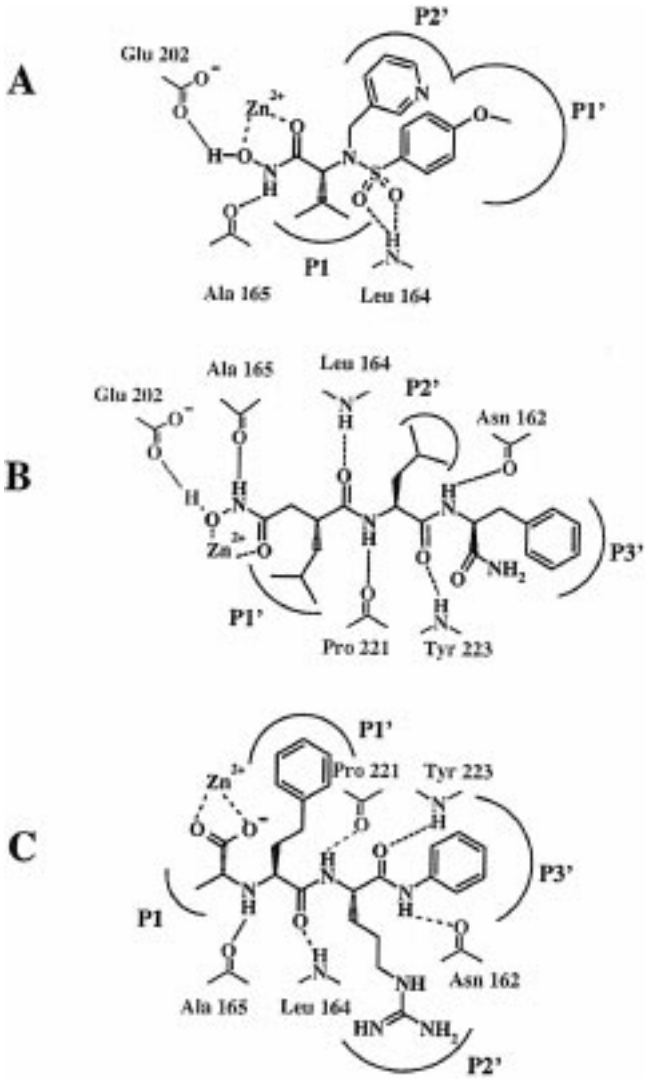


FIGURE 5: Schematic comparison of SCD−inhibitor binding. (A) Hydroxamic acid CGS 27023, $K_i = 0.013$ μM, shows only two hydrogen-bonding interactions with stromelysin. Proposed interaction of hydroxyl oxygen with Glu 202 Oϵ2 is displayed in magenta. (B) Peptidic hydroxamic acid PD-140798, $K_i \sim 0.040$ μM, shows five hydrogen bonds to the enzyme. Although X-ray data suggests a possible protonated state for the inhibitor's hydroxyl oxygen (displayed in gray) (*16*), NMR data supports a nonprotonated state (*17*−*18*). (C) *N*-carboxyalkyl peptide, $K_i \sim 0.23$ μM, shows four hydrogen bonds with stromelysin (*15*, *19*, *20*). A fifth hydrogen bond (∼ 2.88 Å) between Pro 221 and inhibitor (displayed in red) was suggested by the X-ray structure (*15*) as a potential weak hydrogen-bonding interaction.

oxygens (1.96 and 2.24 Å). These hydrogen-bonding interactions were corroborated by deuterium-exchange experiments and subsequently incorporated into the structure refinement calculations. Coordination of both hydroxamate oxygens of the bound inhibitor with the catalytic zinc ion was also readily apparent from the NOE-derived structure which positioned both oxygens for optimal coordination with the catalytic zinc (Figure 4). This ligand−metal coordination was consistent with reported NMR and X-ray structures of SCD−inhibitor complexes (*16*, *18*).

An interesting characteristic of this inhibitor is the tendency for the hydroxyl oxygen on the hydroxamic acid moiety to remain protonated in the bound state. This hydroxyl proton resonates significantly downfield from the other resonances (14.57 ppm) to allow unambiguous iden-

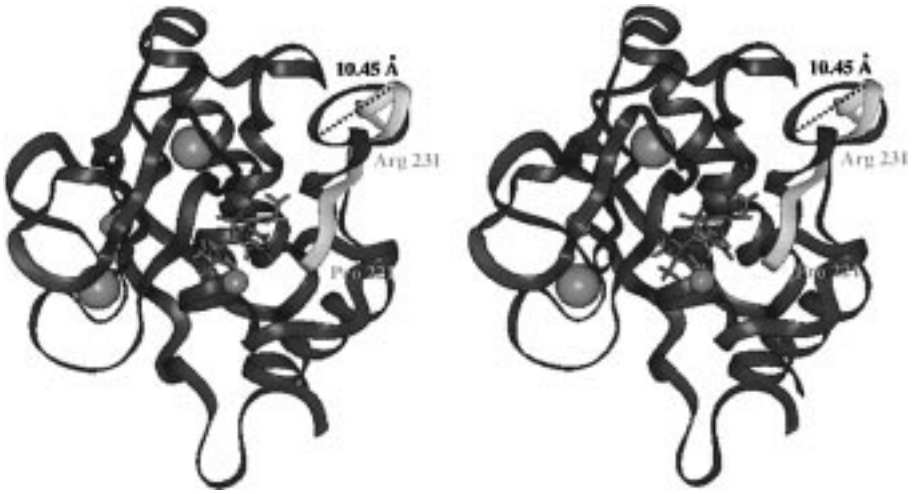


FIGURE 6: Stereoview (relaxed eye) of superimposed ribbon structures of the stromelysin catalytic domain. The SCD−CGS 27023 complex is displayed with the protein backbone in blue, the inhibitor in red, the zinc atoms in purple, and the calcium atoms in orange. The backbone region (residues Phe 221−Arg 231) of the SCD−*N*-carboxyalkyl peptide complex (*20*) is shown in yellow. The illustration shows that the backbone loop region flanking the S1′ pocket can move by as much as 10 Å to accommodate different inhibitors.

tification in the 2D NOESY spectrum. The assignment was corroborated by intermolecular NOEs observed between the inhibitor's hydroxyl proton (1HO) and His 201 (HD2), Glu 202 (HA), and (HG1) as well as intramolecular NOEs between 1HO and 3HD1, HG1* and 1HN (*36*). Examination of the NMR-derived structure revealed that a hydrogen-bonding interaction as well as a protected environment may account for the observed protonation phenomenon. Our NMR data showed that a possible hydrogen bond (∼2.32 Å) can exist between the inhibitor's hydroxyl proton (1HO) and the side chain carboxylate oxygen of Glu 202 (O$\epsilon$2) (Figure 5A). The structure also revealed that the orientation of the inhibitor's isopropyl group introduces a hydrophobic barrier about the hydroxamic acid moiety. This hydrophobic protection factor may strengthen the proposed hydrogen bond between the inhibitor's (1HO) and Glu 202 (O$\epsilon$2) by preventing rapid exchange of the hydroxyl proton with water molecules.

Protonation of the hydroxyl oxygen was not reported for the NMR structure of the peptidic hydroxamic acid (Figure 5B) complexed to SCD (*18*). On the basis of the published structure, this result would not be unexpected since orientation of the bound peptidic inhibitor leaves the hydroxyl proton with no hydrogen-bonding interaction and solvent-exposed. Under such circumstances rapid exchange of this proton with water would be favored. It is interesting that the corresponding X-ray structure of the bound peptidic inhibitor does reveal that a hydrogen-bonding interaction can exist between the inhibitor's hydroxyl proton (1HO) and Glu 202 (O$\epsilon$2); however the absence of a protected environment for the hydroxyl proton preventing rapid exchange with water may serve to weaken the interaction (*16*). Therefore, although structural comparison of the nonpeptidic versus peptidic hydroxamate inhibitors (Figure 5, parts A and B, respectively) reveals that a hydrogen bond can exist in both cases between hydroxyl proton (1HO) and Glu 202 (O$\epsilon$2), the protected environment of the hydroxamic acid for the SCD−CGS 27023 complex may serve to strengthen its hydrogen-bonding interactions and thereby contribute to the overall binding energy of the complex.

The inhibitor used in this study exhibits remarkable potency against stromelysin ($K_i$ = 13 nM) yet makes few hydrogen-bonding or hydrophobic contacts with the enzyme backbone when compared to peptidic inhibitors of similar or reduced potency (*15*, *16*, *18*, *20*). A schematic representation of SCD−inhibitor interactions for CGS 27023 and previously reported peptidic inhibitors is shown in Figure 5. It is interesting that the carboxylate inhibitor (Figure 5C) is about 20-fold less potent than CGS 27023 (Figure 5A), yet has a phenyl group which extends more deeply into the S1′ pocket and makes two additional hydrogen-bonding contacts with the enzyme. This difference may largely be attributed to the expected reduction in potency on going from zinc coordination with an hydroxamic acid to that of a carboxylate. Comparison with the peptidic hydroxamate structure (Figure 5B), however, revealed approximately a 2-fold reduction in potency relative to CGS 27023, even though the peptidic inhibitor formed three additional hydrogen bonds with the enzyme and showed significant hydrophobic interaction from the leucine moiety in S1′. Also unlike CGS 27023, both peptidic inhibitors possessed P2′ and P3′ side chains that were closely associated with the protein. On the basis of these comparisons, it is remarkable that the additional hydrogen-bonding and hydrophobic interactions of the peptidic inhibitors with stromelysin were not required for CGS 27023 binding potency.

*Enzyme Comparison with Other SCD Complexes.* The tertiary fold of the SCD−CGS 27023 complex showed very good agreement with previously reported X-ray and NMR structures (*15*, *19*, *20*). Only the NMR structure obtained in 15% acetonitrile revealed some deviation in the relative orientation of the loop region from residue 150 to residue 163 (*17*, *18*). This deviation was consistent with a previous report comparing the NMR structure in 15% acetonitrile with its corresponding X-ray structure (*16*). While the cause of this discrepancy was not clear, it is possible that the presence of acetonitrile may have been a contributing factor.

Although the secondary structure and overall global fold of the SCD−CGS 27023 complex were virtually identical with published structures, we found some dramatic changes at the enzyme's binding site. One major structural difference for stromelysin was a shift in the orientation of the S1′ loop when complexed to peptidic inhibitors (*15*−*20*) versus our nonpeptidic inhibitor. For the peptidic inhibitors, this shift

in loop orientation was due to hydrogen-bonding interactions with residues Asn 162 (CO), Pro 221 (CO), and Tyr 223 (NH), not found with CGS 27023 (Figure 5). Apparently the loss of 3 hydrogen bonds in the SCD−CGS 27023 complex allows the backbone of the enzyme's flexible loop region to shift by approximately 2 Å to better accommodate the nonpeptidic inhibitor. Another striking feature of this S1′ loop is its ability to undergo a dramatic conformational change. Unlike prior reports with peptidic inhibitors where the loop adopts an open conformation, this loop region folds in upon the long narrow hydrophobic pocket creating a compact structure. NOEs between Asp 189 (NH) and Leu 229 (HD1*), Thr 190 (HA) and Leu 229 (HN), Thr 190 (HA) and Leu 226 (HN), Thr 191 (HN) and Leu 229 (HD1*), Leu 197 (HN) and Thr 227 (HG1), Leu 197 (HN) and Thr 227 (HB), Val 198 (HN) and Thr 227 (HB), and Val 198 (HN) and Thr 227 (HG1) define this structural feature. Comparison of the enzyme's backbone with published structures (*15*, *16*, *18*, *20*) shows that loop Pro 221−Arg 231 can move by as much as 10 Å (Figure 6). Such a conformational change could contribute to the potent binding properties of this inhibitor by producing a compact structure which may partially compensate for the limited enzyme−inhibitor interactions. This conformational fold also produces a structure with lessened accessibility to the long narrow S1′ pocket. On the basis of this structure alone, predictions on the depth and breath of potential S1′ penetration by various inhibitor templates would be compromised.

Because of the significant backbone conformational changes at the enzyme's active site, this study underscores the importance of understanding protein dynamics in inhibitor binding. Our results suggest that incorporation of enzyme dynamics into theoretical docking algorithms can be essential for accurate structure prediction. Such measures to ensure improved sampling of conformational space may reveal binding modes not favorably predicted from a more rigid template. Finally, because enzymes such as stromelysin exhibit binding site flexibility, our results demonstrate a critical need to generate experimental structures for a variety of different inhibitor classes. Only by sampling different inhibitor templates can one appreciate the full range of enzymatic mobility in accommodating novel inhibitor designs.

## CONCLUSIONS

The full three-dimensional structure of the stromelysin catalytic domain complexed to a potent nonpeptidic inhibitor has been solved by NMR spectroscopy. The results showed that although the inhibitor makes few hydrogen-bonding interactions and hydrophobic contacts with the enzyme, it nonetheless retains excellent binding potency. Examination of the enzyme structure on inhibitor binding revealed a conformational change in loop region (Pro 221−Arg 231) extending along the length of the S1′ pocket. This conformational fold of the enzyme to create a compact structure may also contribute to the binding energy by compensating for the reduction in hydrogen-bonding and hydrophobic interactions of our inhibitor relative to its peptidic counterparts. In addition, the binding site flexibility of SCD demonstrates the need for numerous experimental structures to accurately predict binding modes of different inhibitor classes.

## ACKNOWLEDGMENT

The authors wish to thank Dr. David Parker for the inhibitor (CGS 27023), Dr. Michelle Kelly for the mass spectrometry data and analysis, and Dr. Jerry Skiles for critical review of the manuscript.

## SUPPORTING INFORMATION AVAILABLE

Proton chemical shift assignments and distance constraints used in the structure calculations (36 pages) are available. Ordering information is given on any current masthead page.

## REFERENCES

1. Woessner, J. F., Jr. (1991) *FASEB J. 5*, 2145−2154.
2. Birkedal-Hansen, H., Moore, W. G. I., Bodden, M. K., Windsor, L. J., Birkedal-Hansen, B., DeCarlo, A., and Engler, J. A. (1993) *Crit. Rev. Oral Biol. Med. 4*, 197−250.
3. Cawston, T. E. (1996) *Pharmacol. Ther. 70*, 163−182.
4. Powell, W. C., and Matrisian, L. M. (1996) *Curr. Top. Microbiol. Immunol. 213*, 1−21.
5. Murphy, G., Hembry, R. M., and Reynolds, J. J. (1986) *Collagen Relat. Res. 6*, 351−363.
6. Flannery, C., Lark, M. W., and Sandt, J. D. (1992) *J. Biol. Chem. 267*, 1008−1014.
7. Stetler-Stevenson, W. G., Liotta, L. A., and Kleiner, D. E., Jr. (1993) *FASEB J. 7*, 1434−1441.
8. Dollery, C. M., McEwan, J. R., and Henney, A. M. (1995) *Circ. Res. 77*, 863−868.
9. Zempo, N., Koyama, N., Kenagy, R. D., Lea, H. J., and Clowes, A. W. (1996) *Arterioscler. Thromb. 16*, 28−33.
10. Lee, R. T., Schoen, F. J., Loree, H. M., Lark, M. W., and Libby, P. (1996*) Arterioscler. Thromb. 16*, 1070−1073.
11. Zask, A., Levin, J. I., Killar, L. M., and Skotnicki, J. S. (1996) *Curr. Pharm. Des. 2*, 624−661.
12. Marcy, A. I., Eiberger, L. L., Harrison, R., Chan, H. K., Hutchinson, N. I., Hagmann, W. K., Cameron, P. M., Boulton, D. A., and Hermes, J. D. (1991) *Biochemistry 30*, 6476−6483.
13. Van Wart, H., and Birkedal-Hansen, H. (1990) *Proc. Natl. Acad. Sci. U.S.A. 87*, 5578−5582.
14. Ye, Q. Z., Johnson, L. L., Hupe, D. J., and Baragi, V. (1992) *Biochemistry 31*, 11231−11235.
15. Becker, J. W., Marcy, A. I., Rokosz, L. L., Axel, M. G., Burbaum, J. J., Fitzgerald, P. M. D., Cameron, P. M., Esser, C. K., Hagmann, W. K., Hermes, J. D., and Springer, J. P. (1995) *Protein Sci. 4*, 1966−1976.
16. Dhanaraj, V., Ye, Q.-Z., Johnson, L. L., Hupe, D. J., Ortwine, D. F., Dunbar, J. B., Jr., Rubin, R. J., Pavlovsky, A., Humblet, C., and Blundell, T. L. (1996) *Structure 4*, 375−386.
17. Van Doren, S. R., Kurochkin, A. V., Hu, W., Ye, Q., Johnson, L. J., Hupe, D. J., and Zuiderweg, E. R. P. (1993) *Biochemistry 32*, 13109−13122.
18. Van Doren, S. R., Kurochkin, A. V., Hu, W., Ye, Q., Johnson, L. J., Hupe, D. J., and Zuiderweg, E. R. P. (1995) *Protein Sci. 4*, 2487−2498.
19. Gooley, P. R., Johnson, B. A., Marcy, A. I., Cuca, G. C., Salowe, S. P., Hagmann, W. K., Esser, C. K., and Springer, J. P. (1993) *Biochemistry 32*, 13098−13108.
20. Gooley, P. R., O'Connell, J. F., Marcy, A. I., Cuca, G. C., Salowe, S. P., Bush, B. L., Hermes, J. D., Esser, C. K., Hagmann, W. K., Springer, J. P., and Johnson, B. A. (1994) *Nat. Struct. Biol. 1*, 111−118.
21. MacPherson, L. J., and Parker, D. T. (1995) U.S. Patent 5455258.
22. MacPherson, L. J., Bayburt, E. K., Capparelli, M. P., Carroll, B. J., Goldstein, R., Justice, R. J., Zhu, L., Hu, S., Melton, R. A., Fryer, L., Goldberg, R. L., Doughty, R. J., Spirito, S., Blancuzzi, V., Wilson, D., O′Byrne, E. M., Ganu, V., and Parker, D. T. (1997) *J. Med. Chem. 40*, 2525−2532.

23. Niedzwiecki, L., Teahan, J., Harrison, R. K., and Stein, R. L. (1992) *Biochemistry 31,* 12618−12623.
24. Bodenhausen, G., and Ruben, D. J. (1980) *Chem. Phys. Lett. 69*, 185−189.
25. Sklenar, V., and Bax, A. (1987) *J. Magn. Reson. 71*, 379−383.
26. Grzesiek, S., and Bax, A. (1992) *J. Magn. Reson. 99*, 201−207.
27. Grzesiek, S., and Bax, A. (1993) *J. Biomol. NMR. 3*, 185−204.
28. Grzesiek, S., and Bax, A. (1992) *J. Magn. Reson. 96*, 432−440.
29. Vuister, G. W., and Bax, A. (1993) *J. Am. Chem. Soc. 115*, 7772−7777.
30. Bax, A., Clore, G. M., and Gronenborn, A. G. (1990) *J. Magn. Reson. 88*, 425−431.
31. Fesik, S. W., Eaton, H. L., Olejniczak, E. T., Zuiderweg, E. R. P., McIntosh, L. P., and Dahlquist, F. W. (1990) *J. Am. Chem. Soc. 112*, 886−888.
32. Otting, G., and Wuthrich, K. (1990) *Q. Rev. Biophys. 23*, 39−96.
33. Bax, A., Vuister, G. W., Grzesiek, S., Delaglio, F., Wang, A. C., Tschudin, R., and Zhu, G. (1994) *Methods Enzymol. 239*, 79−105.
34. Marion, D., Kay, L. E., Sparks, S. W., Torchia, D. A., and Bax, A. (1989) *J. Am. Chem. Soc. 111*, 1515−1517.
35. Brunger, A. T. (1993) X-PLOR Version 3.1 Yale University Press, New Haven, CT.
36. Gonnella, N. C., Li, Y.-C., Zhang, X., and Paris, C. G. (1997) *Bioorg. Med. Chem.* 5, 2193−2201.
37. Lovejoy, B., Cleasby, A., Hassel, A. M., Longley, K., Luther, M. A., Weigl, D., Mcgeehan, G., McElroy, A. B., Drewry, D., Lambert, M. H., and Jordan, S. R. (1994) *Science 263*, 375−377.
38. Willenbrock, F., Murphy, G., Phillips, I. R., and Brocklehurst, K. (1995) *FEBS Lett. 358*, 189−192.
39. Laskowski, R. A., MacArthur, M. W., Moss, D. S., and Thornton, J. M. (1993) *J. Appl. Crystallogr. 26*, 283−291.

BI981328W